

# Multiobjective Hybrid Optimization-Antioptimization for Force Design of Tensegrity Structures

**Makoto Ohsaki\***

Professor  
Dept. of Architecture  
Hiroshima University  
1-4-1, Kagamiyama  
Higashi-Hiroshima 739-8527, Japan  
Email: ohsaki@hiroshima-u.ac.jp

**Jingyao Zhang**

Lecturer  
Dept. of Architecture and Urban Design  
Ritsumeikan University, Japan  
Email: zhang@fc.ritsumei.ac.jp

**Isaac Elishakoff**

Professor, Member of ASME  
Dept. of Ocean and Mechanical Engineering  
Florida Atlantic University  
Email: elishako@fau.edu

## ABSTRACT

*Properties of Pareto optimal solutions considering bounded uncertainty are first investigated using an illustrative example of a simple truss. It is shown that the nominal values of the Pareto optimal solutions considering uncertainty are slightly different from those without considering uncertainty. A hybrid approach of multiobjective optimization and antioptimization is next presented for force design of tensegrity structures. We maximize the lowest eigenvalue of the tangent stiffness matrix and minimize the deviation of forces from the specified target distribution. These objective functions are defined as the worst values due to the possible errors in the fabrication and construction processes. The Pareto optimal solutions are found by solving the two-level optimization-antioptimization problems using a nonlinear programming approach for the upper optimization problem and enumeration of the vertices of the uncertain region for the lower antioptimization problem.*

## 1 Introduction

A tensegrity structure consists of cables and struts that can transmit only tensile and compressive forces, respectively [1, 2], which is called stress unilateral property. Tensegrity structures are used as the components of mechanical and aeronautical structures [3–5] and the models of biomechanical systems [6, 7]. Since the tensegrity structure is unstable in absence of prestresses, the shape and stability at the self-equilibrium state strongly depend on the member forces that are defined as the linear combination of the modes of prestress [8–11]. Hence, for a structure consisting of several independent modes of prestress, the stiffness against external loads is desirable to be maximized by optimization of the coefficients of the prestress modes.

The process of determination of member forces for the tensegrity structure with given shape is called *force design* [12], where the prestresses are to be assigned considering the equilibrium conditions and stress unilateral properties. Bounds for tensile and compressive forces should also be given appropriately to have enough safety against yielding and buckling. Since these bounds are expressed as linear inequality constraints with respect to the coefficients of the independent modes of self-equilibrium forces, the set of feasible, or admissible, coefficients is given as a convex region bounded by hyperplanes of the coefficients.

---

\*Address all correspondence related to this paper to this author.

In the practical design process, the forces of cables and struts are appropriately measured and controlled so that the deviations from the nominal values are within the specified bounds. However, the nodal locations are first adjusted by sacrificing the accuracy of the forces so as to realize the structural shape that is determined to ensure the target function of the structure. This process is consistent to the fact that the nodal locations are fixed in the process of force design. Therefore, inevitable error exists in member forces from the nominal values due to errors in fabrication and construction processes. Although errors also exist in the nodal locations, moderately large errors in nodal locations do not lead to serious deviations in mechanical properties as demonstrated in the numerical examples. Therefore, in this paper, only uncertainty in member forces is considered, and the region of uncertainty of the forces is defined as a convex region of the coefficients of the self-equilibrium force modes.

There have been several optimization approaches developed for force design of tensegrity structures [10,13]. Mechanical properties such as the lowest eigenvalue of tangent stiffness matrix and the compliance against specified static loads are considered as objective and/or constraint functions. If we incorporate uncertainty in the variables and parameters, then the objective and/or constraint functions should be defined as the antioptimal solutions [14] or the worst-case designs, and the problem turns out to be a hybrid *optimization–antioptimization* problem [15]. Suppose we maximize a concave function of the coefficients for the self-equilibrium modes. Then, the antioptimal solution that *minimizes* the concave function can be found by enumerating the vertices of the convex region [16, 17].

Another important aspect of practical force design is that multiple performance measures should be considered; hence, the problem turns out to be a multiobjective programming (MOP) problem [18, 19]. Although numerous works exist for antioptimization for finding the worst-case design, multiobjective optimization with nonprobabilistic bounded uncertainty has been mainly investigated in the field of fuzzy-set-based theory [20,21], and no detailed investigation has been made in the framework of standard nonlinear programming (NLP) problem. Rao [22] defined an M-Pareto optimal solution in the space of membership functions of fuzzy theory, and proposed an approach that is similar to a goal programming. Loetamonphong *et al.* [23] used a genetic algorithm for generating Pareto optimal set. Some applications of the fuzzy-set-based approach are found for tunneling reinforcement design [24] and planning of water resource system [25].

In this paper, the properties of Pareto optimal solutions considering worst-case scenario are first investigated in detail for a simple truss subjected to static loads. The design variables are the cross-sectional area, and the uncertain region of the height is defined as an interval. It is shown through the optimality conditions that the same set of Pareto optimal solutions is obtained using the linear-weighted-sum approach and the constraint approach in the similar manner as the case without uncertainty in the parameters. It is important to note here that the nominal values of Pareto optimal solutions considering uncertainty are different from the Pareto solutions without uncertainty.

We next present a multiobjective hybrid optimization–antioptimization method for force design of tensegrity structures [26]. The member forces are defined as a linear combinations of the self-equilibrium force modes. The coefficients of the force modes are optimized for maximization of the lowest eigenvalue of the tangent stiffness matrix and minimization of the deviation of forces from the target values. In the numerical examples, following an example of a simple tensegrity structure, a set of Pareto optimal solutions are found for a tensegrity grid that has four self-equilibrium force modes. Since the lowest eigenvalue is concave and the force deviation is convex with respect to the coefficients for the force modes, the worst-case solutions are found by enumeration of vertices of the convex region of uncertainty. A hybrid approach is presented as a combination of NLP and vertex enumeration, respectively, for optimization and antioptimization, where the linear-weighted-sum approach is used for finding a set of Pareto optimal solutions.

## 2 Multiobjective hybrid optimization–antioptimization problem

When an MOP problem is solved using an NLP approach, the problem is transformed to a single-objective problem using a method of scalarization; e.g., linear-weighted-sum approach, constraint approach, and goal programming [19]. Since it is not generally possible to find an optimal solution that minimizes all objective functions simultaneously, a compromise solution is regarded as a solution to an MOP problem. A feasible solution satisfying all the constraints is called Pareto optimal solution, if there exists no other feasible solution that simultaneously improves all the objective functions [18]. However, it is not straightforward to see if the sets of Pareto optimal solutions obtained using different approaches of MOP are the same, when uncertainty exists in the variables and/or parameters.

As an illustrative example, consider a problem of minimizing the total structural volume and compliance (external work) of a truss subjected to static loads. Let  $\mathbf{A}$  denote the vector of cross-sectional areas of a truss. The lower and upper bounds for  $\mathbf{A}$  are denoted by  $\mathbf{A}^L$  and  $\mathbf{A}^U$ , respectively. The problem of minimizing the total structural volume  $V(\mathbf{A})$  and the compliance  $W(\mathbf{A})$  is formulated as

$$\text{Minimize } V(\mathbf{A}) \text{ and } W(\mathbf{A}) \quad (1a)$$

$$\text{subject to } \mathbf{A}^L \leq \mathbf{A} \leq \mathbf{A}^U \quad (1b)$$

Suppose we have a parameter vector  $\mathbf{p}$ , for which the range of uncertainty is specified by the interval:

$$\mathbf{p}^L \leq \mathbf{p} \leq \mathbf{p}^U \quad (2)$$

The set of  $\mathbf{p}$  satisfying (2) is denoted by  $\mathcal{P}$ . The hybrid MOP problem of minimizing the objective functions corresponding to the worst parameter values is formulated as follows:

$$\text{Minimize } \max_{\mathbf{p} \in \mathcal{P}} V(\mathbf{A}, \mathbf{p}) \text{ and } \max_{\mathbf{p} \in \mathcal{P}} W(\mathbf{A}, \mathbf{p}) \quad (3a)$$

$$\text{subject to } \mathbf{A}^L \leq \mathbf{A} \leq \mathbf{A}^U \quad (3b)$$

where the variables for minimization are  $\mathbf{A}$ .

Since the worst values of  $V$  and  $W$  with respect to  $\mathbf{p}$  can be conceived as functions of  $\mathbf{A}$  only, they are denoted with tilde as  $\tilde{V}(\mathbf{A})$  and  $\tilde{W}(\mathbf{A})$ , respectively. Hence, the problem is rewritten as

$$\text{Minimize } \tilde{V}(\mathbf{A}) \text{ and } \tilde{W}(\mathbf{A}) \quad (4a)$$

$$\text{subject to } \mathbf{A}^L \leq \mathbf{A} \leq \mathbf{A}^U \quad (4b)$$

Therefore, the hybrid problem can be formally formulated as a standard MOP problem, and the Pareto optimal solutions can be obtained using any method of scalarization. For example, if we use the constraint approach and linear-weighted-sum approach, we have the following problems, respectively:

Constraint approach:

$$\text{P1 : Minimize } \tilde{V}(\mathbf{A}) \quad (5a)$$

$$\text{subject to } \mathbf{A}^L \leq \mathbf{A} \leq \mathbf{A}^U \quad (5b)$$

$$\tilde{W}(\mathbf{A}) \leq W^U \quad (5c)$$

$$\text{P2 : Minimize } \tilde{W}(\mathbf{A}) \quad (6a)$$

$$\text{subject to } \mathbf{A}^L \leq \mathbf{A} \leq \mathbf{A}^U \quad (6b)$$

$$\tilde{V}(\mathbf{A}) \leq V^U \quad (6c)$$

Linear-weighted-sum approach:

$$\text{P3 : Minimize } C_1 \tilde{V}(\mathbf{A}) + C_2 \tilde{W}(\mathbf{A}) \quad (7a)$$

$$\text{subject to } \mathbf{A}^L \leq \mathbf{A} \leq \mathbf{A}^U \quad (7b)$$

where  $V^U$  and  $W^U$  are the upper bounds for  $V$  and  $W$ , respectively, which are the parameters for the constraint approach, and  $C_1$  and  $C_2$  are the positive weight coefficients.

In the following, the Pareto optimal solutions are found analytically for a 2-bar truss as shown in Fig. 1. For simplicity, the units are omitted as  $S = 2.0$ ,  $P_1 = P_2 = 1.0$ , and the elastic modulus is  $E = 1.0$ . Consider uncertainty in  $H$  defined by an interval

$$H_0 - \Delta H \leq H \leq H_0 + \Delta H \quad (8)$$

where the nominal value  $H_0$  and the radius of interval  $\Delta H$  are given as  $H_0 = 1.0$  and  $\Delta H = 0.4$ , respectively. The compliance  $W$  is defined using the horizontal displacement  $U_1$  and the vertical displacement  $U_2$  as

$$W = P_1 U_1 + P_2 U_2 \quad (9)$$

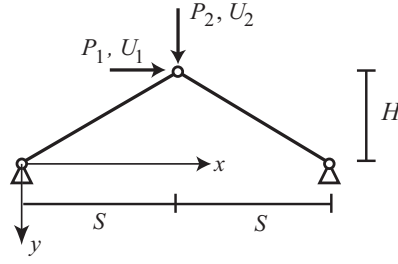


Fig. 1. A two-bar truss.

The design variables are  $\mathbf{A} = (A_1, A_2)$ , and the components of  $\mathbf{A}^L$  and  $\mathbf{A}^U$  are supposed to be sufficiently small and large, respectively. Hence, the bound constraints  $\mathbf{A}^L \leq \mathbf{A} \leq \mathbf{A}^U$  are inactive at the optimal solution, i.e., they are satisfied with strict inequality. Accordingly, the constraints (5c) and (6c) are satisfied with equality at the optimal solutions, which generally holds because  $\tilde{V}(\mathbf{A})$  and  $\tilde{W}(\mathbf{A})$  are increasing and nonincreasing functions, respectively, of  $\mathbf{A}$ .

In the following, analytical expressions are derived using a symbolic computation package Maple 13 [27]. The displacements  $U_1$  and  $U_2$  are written explicitly with respect to the cross-sectional areas with parameter  $H$  as

$$U_1 = \frac{aH}{2} [b(4 + H^2) + 2c] \quad (10a)$$

$$U_2 = a [b(4 + 4H + H^3) + 4cH] \quad (10b)$$

$$a = \frac{(4 + H^2)^{3/2}}{8A_1A_2H^2} \quad (10c)$$

$$b = A_1 + A_2, \quad c = A_1 - A_2 \quad (10d)$$

As verified below, the worst (maximum) value of  $W$  is attained at  $H = H_0 - \Delta H$ . In contrast,  $V$  obviously has the worst (maximum) value at  $H = H_0 + \Delta H$ . Therefore, the antioptimal solutions for maximizing  $W$  and  $V$ , respectively, can be obtained analytically as functions of  $\mathbf{A}$ ; hence, the worst values  $\tilde{W}$  and  $\tilde{V}$  are written as the explicit functions of  $\mathbf{A}$ . Then, for P1 and P2,  $A_2$  can be eliminated using the constraints (5c) and (6c), respectively, which are to be satisfied with equality at the optimal solution. The optimal solutions are found from the stationary conditions of the objective functions with respect to  $A_1$ . For P3, the optimal solutions are found from the stationary conditions of the objective function with respect to  $A_1$  and  $A_2$ .

This way, the optimal solutions for problems P1, P2, and P3 are obtained explicitly as follows:

$$\begin{aligned} \text{P1: } & A_1 = 8.8511/W^U, \quad A_2 = 16.44/W^U, \\ & V = 61.74/W^U, \quad W = W^U \\ \text{P2: } & A_1 = 0.1434V^U, \quad A_2 = 0.2663V^U, \\ & V = V^U, \quad W = 61.74/V^U \\ \text{P3: } & A_1 = 1.127\sqrt{C_2/C_1}, \quad A_2 = 2.092\sqrt{C_2/C_1}, \\ & V = 7.857\sqrt{C_2/C_1}, \quad W = 7.857\sqrt{C_2/C_1} \end{aligned} \quad (11)$$

Although the expressions of the solutions are different, three solutions lead to the same set of Pareto optimal solutions satisfying

$$A_2 = 1.857A_1, \quad WV = 61.74 \quad (12)$$

This result is justified from the fact that three problems have the same optimality conditions. Let  $\mu$  and  $\nu$  denote the Lagrange

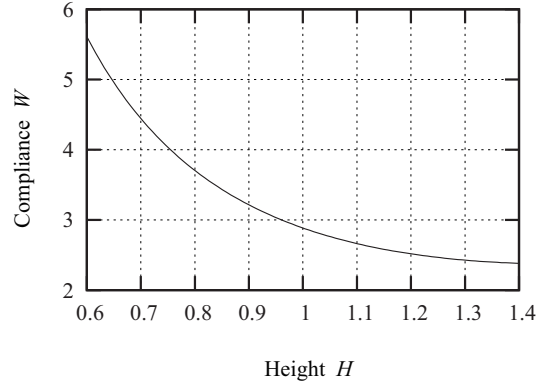


Fig. 2. Relation between  $H$  and  $W$  for the design  $A_1 = 1.0$  and  $A_2 = 1.857$ .

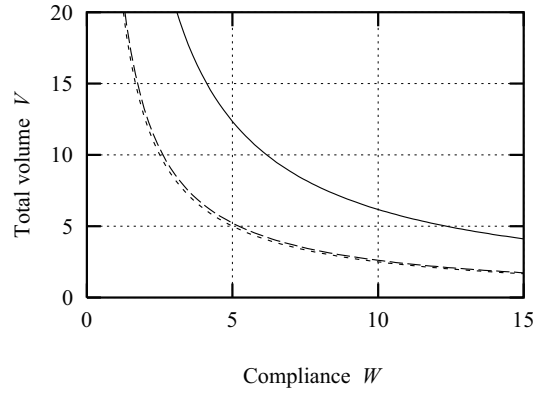


Fig. 3. Relations between  $W$  and  $V$  of Pareto optimal solutions; dotted line: solutions without uncertainty, solid line: solutions with uncertainty, dashed line: nominal values of the solutions with uncertainty.

multipliers. The optimality conditions for P1, P2, and P3 are written as

$$P1 : \frac{\partial \tilde{V}}{\partial A_i} + \mu \frac{\partial \tilde{W}}{\partial A_i} = 0, \quad (i = 1, 2) \quad (13a)$$

$$P2 : \frac{\partial \tilde{W}}{\partial A_i} + v \frac{\partial \tilde{V}}{\partial A_i} = 0, \quad (i = 1, 2) \quad (13b)$$

$$P1 : C_1 \frac{\partial \tilde{V}}{\partial A_i} + C_2 \frac{\partial \tilde{W}}{\partial A_i} = 0, \quad (i = 1, 2) \quad (13c)$$

These equations are identical if the multipliers are found as

$$\frac{1}{\mu} = v = \frac{C_1}{C_2} \quad (14)$$

Fig. 2 shows the relation between  $W$  and  $H$  for the design  $A_1 = 1.0$  and  $A_2 = 1.857$ , which verifies that  $W$  is a decreasing function of  $H$ , and, accordingly, has the worst (maximum) value at  $H = H - \Delta H$ . The solid line in Fig. 3 shows the relation between the worst values of  $W$  and  $V$  of the Pareto optimal solutions. The relation between the nominal values of  $W$  and  $V$  of the Pareto optimal solutions is plotted in the dashed line in Fig. 3, which satisfies the relation  $WV = 26.10$ , which is much smaller than the worst value 61.74 in (12). Furthermore, if uncertainty is not considered, the relation between  $W$  and  $V$  of the Pareto optimal solutions is as plotted in the dotted line, which satisfies the relation  $WV = 25.00$ . Therefore, even the nominal values of  $W$  and  $V$  of the Pareto solutions increase due to the existence of uncertainty. This fact can be theoretically justified from the fact that the solution of P1 (or P2) is a feasible solution of the problem without uncertainty for specified value of  $W^U$  (or  $V^U$ ), and does not always satisfy the optimality conditions of the problem without uncertainty. Therefore, optimization without uncertainty does not provide any information on optimization with uncertainty.

### 3 Equilibrium and stiffness of tensegrity structures

In the numerical examples, Pareto optimal solutions are found for the coefficients of self-equilibrium forces of a tensegrity grid. The members, including struts and cables, are connected by pin joints, and the self-weight is neglected; hence, only axial forces exist in the members. We assume that all members are in elastic range, and neither buckling nor yielding is considered.

Let  $m$  and  $n$  denote the numbers of members and degrees of freedom, respectively. The  $n \times m$  equilibrium matrix  $\mathbf{D}$  is constructed using the standard approach for 3-dimensional bar-joint structures. The vector of member forces is denoted by  $\mathbf{s}$ . In the state of self-equilibrium, the equilibrium equation is written as

$$\mathbf{D}\mathbf{s} = \mathbf{0} \quad (15)$$

Let  $\kappa$  denote the rank of  $\mathbf{D}$ . The equilibrium equation (15) has  $q = m - \kappa$  self-equilibrium modes, which are found, as follows, by using the singular value decomposition of  $\mathbf{D}$ .

The non-zero eigenvalues of  $\mathbf{D}^\top \mathbf{D}$  are denoted by  $\omega_i$  ( $i = 1, \dots, \kappa$ ). The singular value decomposition of  $\mathbf{D}$  is written as [28]

$$\mathbf{D} = \mathbf{S}^\top \mathbf{D} \mathbf{R} \quad (16)$$

where

$$\mathbf{D} = \begin{pmatrix} \text{diag}(\omega_1, \dots, \omega_\kappa) & \mathbf{O} \\ \mathbf{O} & \mathbf{O} \end{pmatrix} \quad (17)$$

with  $\mathbf{O}$  being null matrix, and the diagonal terms of  $\mathbf{D}$  are called singular values of  $\mathbf{D}$ . The column vectors  $\mathbf{R}_i$  ( $i = \kappa + 1, \kappa + 2, \dots, m$ ) of  $\mathbf{R}$  corresponding to zero singular value satisfy the condition of self-equilibrium force mode as

$$\mathbf{D}\mathbf{R}_i = \mathbf{0} \quad (18)$$

By denoting  $\mathbf{g}_i = \mathbf{R}_{i+\kappa}$  ( $i = 1, \dots, q$ ), the self-equilibrium force vector  $\mathbf{s}$  satisfying  $\mathbf{D}\mathbf{s} = \mathbf{0}$  is given as the linear combination of  $\mathbf{g}_i$  as

$$\begin{aligned} \mathbf{s} &= \alpha_1 \mathbf{g}_1 + \dots + \alpha_q \mathbf{g}_q \\ &= \mathbf{G}\boldsymbol{\alpha} \end{aligned} \quad (19)$$

where  $\boldsymbol{\alpha} = (\alpha_1, \dots, \alpha_q)^\top$  is the coefficient vector, and  $\mathbf{G} = (\mathbf{g}_1, \dots, \mathbf{g}_q)$  is the matrix of the self-equilibrium force modes. Let  $\mathbf{b}_i^\top$  denote the  $i$ th row of  $\mathbf{G}$ . The components of  $\mathbf{s}$  are written as

$$s_i = \mathbf{b}_i^\top \boldsymbol{\alpha}, \quad (i = 1, \dots, m) \quad (20)$$

The tangent stiffness matrix  $\mathbf{K}$  of a tensegrity structure is expressed as the sum of the linear stiffness matrix  $\mathbf{K}_E$  and the geometrical stiffness matrix  $\mathbf{K}_G$  as [12]

$$\mathbf{K} = \mathbf{K}_E + \mathbf{K}_G \quad (21)$$

Note that  $\mathbf{K}_E$  depends on the stiffnesses of members, and  $\mathbf{K}_G$  depends on the member forces.

In the following discussions on stiffness of the structure, the rigid-body motions are assumed to be constrained. Let  $\lambda_r$  ( $\lambda_1 \leq \lambda_2 \leq \dots \leq \lambda_n$ ) and  $\Phi_i$  denote the  $i$ th eigenvalue and eigenvector of  $\mathbf{K}$ , respectively, which are defined by

$$\mathbf{K}\Phi_i = \lambda_i \Phi_i, \quad (i = 1, \dots, n) \quad (22)$$

When the external loads applied to a structure are unknown, the best way to strengthen the structure may be to increase its stiffness in the weakest direction. Hence, the lowest eigenvalue  $\lambda_{\min}$  after constraining the rigid-body motions is maximized as the performance measure in the optimization problem defined in the next section.

#### 4 Multiobjective hybrid optimization–antioptimization problem

The upper and lower bounds for the forces of the  $i$ th member are denoted by  $s_i^U$  and  $s_i^L$ , respectively. The conditions for the member forces are written as

$$s_i^L \leq s_i \leq s_i^U, \quad (i = 1, \dots, m) \quad (23)$$

For a cable,  $s_i^U$  is given as the yield force divided by the associated safety factor, while a small positive value  $s_i^L$  is given for preventing slackening. In contrast, for a strut,  $s_i^L$  is given as the Euler buckling force, which is negative, divided by the safety factor, while  $s_i^U$  may be zero or a negative value with sufficiently small absolute value.

In the process of force design, the geometry (nodal locations) and the topology of the structure are specified. Therefore, the design variables are the coefficients  $\alpha$  for the self-equilibrium modes. By using the relation (20), the constraints for the optimization problems are given with respect to  $\alpha$  as

$$s_i^L \leq \mathbf{b}_i^\top \alpha \leq s_i^U, \quad (i = 1, \dots, m) \quad (24)$$

Let  $\mathbf{s}^*$  denote the target values of the member forces, which can be specified based on the yield forces of cables and buckling forces of struts, or, alternatively, we can use any optimization approaches for defining  $\mathbf{s}^*$  based on other design criteria. In the following antioptimization problem, the deviation  $e$  of the forces from  $\mathbf{s}^*$  is chosen as one of the performance measures, which is defined as follows as a convex function of  $\alpha$ :

$$\begin{aligned} e &= (\mathbf{s}^* - \mathbf{G}\alpha)^\top (\mathbf{s}^* - \mathbf{G}\alpha) \\ &= \mathbf{s}^{*\top} \mathbf{s}^* - 2\mathbf{s}^{*\top} \mathbf{G}\alpha + \alpha^\top \mathbf{G}^\top \mathbf{G}\alpha \end{aligned} \quad (25)$$

Furthermore, the lowest eigenvalue  $\lambda_{\min}$  of  $\mathbf{K}$  after constraining the rigid-body motions is maximized, i.e.,  $-\lambda_{\min}$  is minimized, as the global measure of stiffness and stability of the structure. Note in (21) that  $\mathbf{K}_G$  depends linearly on  $\alpha$ , while  $\mathbf{K}_E$  is independent of  $\alpha$ ; hence,  $\lambda_{\min}$  is a concave function of  $\alpha$  [29]. Then, the MOP problem is formulated as

$$\text{Minimize } -\lambda_{\min}(\alpha) \text{ and } e(\alpha) \quad (26a)$$

$$\text{subject to } s_i^L \leq \mathbf{b}_i^\top \alpha \leq s_i^U, \quad (i = 1, \dots, m) \quad (26b)$$

Consider uncertainty in member forces at the self-equilibrium state due to the errors in unstressed (initial) lengths of members or variation in member lengths resulting from relaxation of cables after construction. In the process of designing tensegrity structures, the errors exist also in the nodal locations. However, the locations of nodes are usually adjusted by sacrificing the accuracy of member forces, which means that the small dislocation of nodes and/or small error in member length leads to variation of mechanical properties only through errors in the member forces. Therefore, in this paper, only uncertainty in member forces is considered.

Since the member force vector  $\mathbf{s}$  should satisfy the self-equilibrium equation (15), the errors in  $\mathbf{s}$  cannot be distributed independently. The equilibrium matrix  $\mathbf{D}$  is fixed, because we do not consider the errors in nodal locations. Therefore, the vectors  $\mathbf{g}_i$  of the self-equilibrium force modes are fixed, and the variation of the member forces is investigated in the space of the coefficient vector  $\alpha$ .

To describe the realistic situation, we assign the range of uncertainty of  $\mathbf{s}$  as an interval

$$s_i^0 - \Delta s_i \leq s_i \leq s_i^0 + \Delta s_i \quad (27)$$

where  $\mathbf{s}^0 = (s_1^0, \dots, s_m^0)^\top$  is the vector of nominal values, and  $\Delta s_i$  is the maximum possible increase or decrease of  $s_i$ . Note that the range is given for the forces  $s_i$ , although the independent parameters for the forces are  $\alpha$ . The inequalities (27) can be rewritten using the increment  $\Delta\alpha$  from the nominal values as

$$-\Delta s_i \leq \mathbf{b}_i^\top \Delta\alpha \leq \Delta s_i, \quad (i = 1, \dots, m) \quad (28)$$

The worst values are obtained by solving the following antioptimization problems:

$$\text{Find } \tilde{\lambda}_{\min}(\alpha) = \min_{\Delta\alpha} \lambda_{\min}(\alpha, \Delta\alpha) \quad (29a)$$

$$\text{subject to } -\Delta s_i \leq \mathbf{b}_i^\top \Delta\alpha \leq \Delta s_i, \quad (i = 1, \dots, m) \quad (29b)$$

$$\text{Find } \tilde{e}(\boldsymbol{\alpha}) = \max_{\Delta\boldsymbol{\alpha}} e(\boldsymbol{\alpha}, \Delta\boldsymbol{\alpha}) \quad (30a)$$

$$\text{subject to } -\Delta s_i \leq \mathbf{b}_i^\top \Delta\boldsymbol{\alpha} \leq \Delta s_i, \quad (i = 1, \dots, m) \quad (30b)$$

Finally, the MOP problem considering the worst values of the performance measures is formulated as

$$\text{Minimize } -\tilde{\lambda}_{\min}(\boldsymbol{\alpha}) \text{ and } \tilde{e}(\boldsymbol{\alpha}) \quad (31a)$$

$$\text{subject to } s_i^L \leq \mathbf{b}_i^\top \boldsymbol{\alpha} \leq s_i^U, \quad (i = 1, \dots, m) \quad (31b)$$

It is widely recognized that the constraint approach is superior to the linear-weighted-sum approach, because the constraint approach can find Pareto optimal solutions even when they exist along the nonconvex boundary of feasible region in the objective function space. However, the location of vertex that has the worst value of an objective function in the antioptimization problem may vary discontinuously with variation of the design variables  $\boldsymbol{\alpha}$ , and it is very difficult to satisfy the constraints strictly for a problem with discontinuous sensitivity coefficients. Therefore, we use the linear-weighted-sum approach in the following examples, and confirm that the Pareto optimal solutions exist along the convex boundary of feasible region. Optimal solutions are first found for single-objective problems for minimizing  $-\tilde{\lambda}_{\min}(\boldsymbol{\alpha})$  and  $\tilde{e}(\boldsymbol{\alpha})$ , respectively. The objective function  $F(\boldsymbol{\alpha})$  for the linear-weighted-sum approach is given as

$$F(\boldsymbol{\alpha}) = -\frac{C}{\delta_\lambda} \tilde{\lambda}_{\min}(\boldsymbol{\alpha}) + \frac{(1-C)}{\delta_e} \tilde{e}(\boldsymbol{\alpha}) \quad (32)$$

where  $\delta_\lambda$  and  $\delta_e$  are the range of  $\tilde{\lambda}_{\min}$  and  $\tilde{e}$ , respectively, obtained from the optimal values of the single-objective problems, and  $0 \leq C \leq 1$  is the weight coefficient.

Since  $\lambda_{\min}$  and  $e$  are concave and convex functions, respectively, the worst values of  $\Delta\boldsymbol{\alpha}$  that minimizes  $\lambda_{\min}$  and maximizes  $e$  exist at the vertices of the region of uncertainty defined by (28). In the following numerical examples, the vertices of the feasible region are enumerated using the software cdd+ [30, 31] based on the efficient procedure called *reverse search* [32]. cdd+ can enumerate the vertices and the associated active constraints of the region defined by linear inequality and equality constraints. Finally, the optimization problem (31) is solved using an NLP approach. The algorithm of multiobjective hybrid optimization and antioptimization is summarized as follows:

- Step 1** Specify the geometry, topology, and material property of the tensegrity structure. Assign the upper bound  $\mathbf{s}^U$  and lower bound  $\mathbf{s}^L$  of the forces, and the radius  $\Delta\mathbf{s}$  of uncertainty.
- Step 2** Construct the equilibrium matrix  $\mathbf{D}$  and compute the self-equilibrium force modes  $\mathbf{g}_1, \dots, \mathbf{g}_q$  by using the singular value decomposition (16).
- Step 3** Assign bound constraints (23) for the self-equilibrium forces and solve the optimization problem of forces using an NLP as follows:
  - 3.1** Set initial value of  $\boldsymbol{\alpha}$ , and assign parameters for NLP.
  - 3.2** Compute the sensitivity coefficients of the objective functions using a finite difference approach, and update the variable  $\boldsymbol{\alpha}$  based on the algorithm of NLP, where the worst values of  $\lambda_{\min}$  and  $e$  are obtained using vertex enumeration at every trial that results in modification of variables.
  - 3.3** Go to 3.2 if convergence criteria of NLP are not satisfied.

We use SNOPT Ver. 7.2 [33] that utilizes the sequential quadratic programming for the upper-level optimization problem. In the following examples, optimization is carried out from ten different random initial solutions, and the best solution is chosen as the optimal solution.

## 5 Numerical examples

### 5.1 Parameters for numerical examples

We first present an illustrative example of a simple tensegrity structure with two self-equilibrium modes to graphically present the optimization process. A numerical example of a tensegrity grid is then presented for demonstrating applicability of the proposed method to general tensegrity structures.

The elastic modulus is  $2000.0 \text{ N/mm}^2$  for all members. The cross-sectional areas are  $50 \text{ mm}^2$  for struts including the bars without prestress, and  $5 \text{ mm}^2$  for cables. The radius of uncertainty  $\Delta s_i$  for member force is  $0.5 \text{ N}$  for all members. In the following, the units of length and force are mm and N, respectively, which are omitted for simplicity.

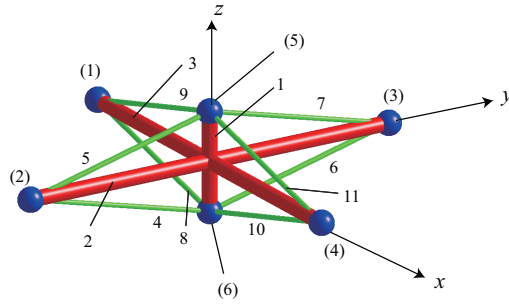


Fig. 4. A simple tensegrity structure.

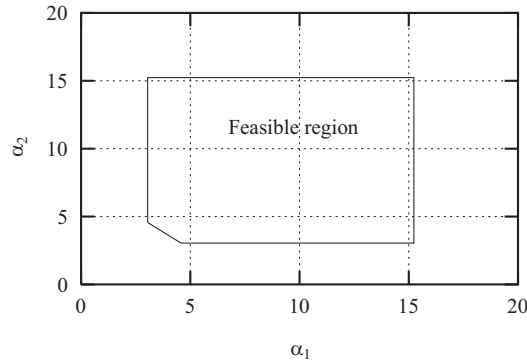


Fig. 5. Feasible region of the coefficients of self-equilibrium force vectors of the small tensegrity structure.

## 5.2 Illustrative example

Consider a simple tensegrity structure as shown in Fig. 4, which has eight cables, one vertical strut, and two horizontal struts. The thick and thin lines in Fig. 4 indicate struts and cables, respectively. Note that the struts are not connected with each other at their centers. The numbers with and without parentheses are the node (support) numbers and member numbers, respectively. The  $(x, y, z)$ -coordinates of the nodes 1–6 are  $(-100, 0, 0)$ ,  $(0, -100, 0)$ ,  $(0, 100, 0)$ ,  $(100, 0, 0)$ ,  $(0, 0, 40)$ , and  $(0, 0, -40)$ , respectively. The structure is supported in three directions at support 1, in  $z$ -direction at support 2, in  $x$ - and  $z$ -directions at support 3, and in  $y$ - and  $z$ -directions at support 4. This way, all the rigid-body displacements are suppressed. The bounds  $(s_i^L, s_i^U)$  for the axial forces of the cables and struts are  $(1, 100)$  and  $(-100, -20)$ , respectively.

The matrix  $\mathbf{G}$  of the self-equilibrium forces is obtained as follows with an appropriate normalization:

$$\mathbf{G} = \begin{pmatrix} -0.2626 & -0.2626 \\ -0.6565 & 0.0 \\ 0.0 & -0.6565 \\ 0.3536 & -0.0 \\ 0.3536 & -0.0 \\ 0.3536 & -0.0 \\ 0.3536 & -0.0 \\ 0.0 & 0.3536 \\ 0.0 & 0.3536 \\ 0.0 & 0.3536 \\ 0.0 & 0.3536 \end{pmatrix} \quad (33)$$

Therefore, we have two self-equilibrium force vectors that have non-zero prestresses in the members in two vertical planes, respectively, and there is an interaction only in the vertical strut indicated as member 1. The feasible region of  $\alpha$  is given by the five vertices  $(\alpha_1, \alpha_2) = (3.0465, 4.5697)$ ,  $(4.5697, 3.0465)$ ,  $(15.232, 3.0465)$ ,  $(15.232, 15.232)$ , and  $(3.0465, 15.232)$  as illustrated in Fig. 5. It is supposed that the target axial force vector  $\mathbf{s}^*$  is defined by the coefficient vector  $\alpha^* = (10.0, 10.0)^\top$ .

First, we find the Pareto optimal solutions without uncertainty in the member forces. The values of  $(\lambda_{\min}, e)$  for the single objective optimization problems for maximizing  $\lambda_{\min}$  and minimizing  $e$ , respectively, are  $(0.14979, 58.534)$  and  $(9.8392 \times$

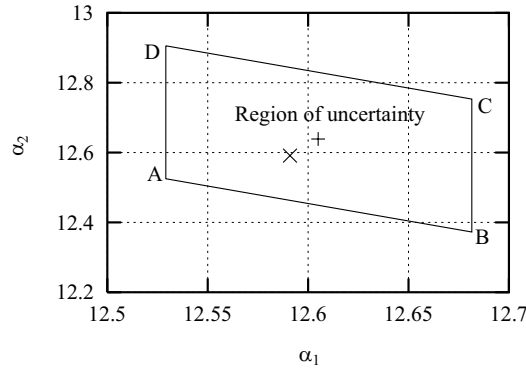


Fig. 6. Pareto optimal solutions for  $C = 0.5$  and the region of uncertainty; '+': Pareto optimal solution with uncertainty, 'x': Pareto optimal solution without uncertainty.

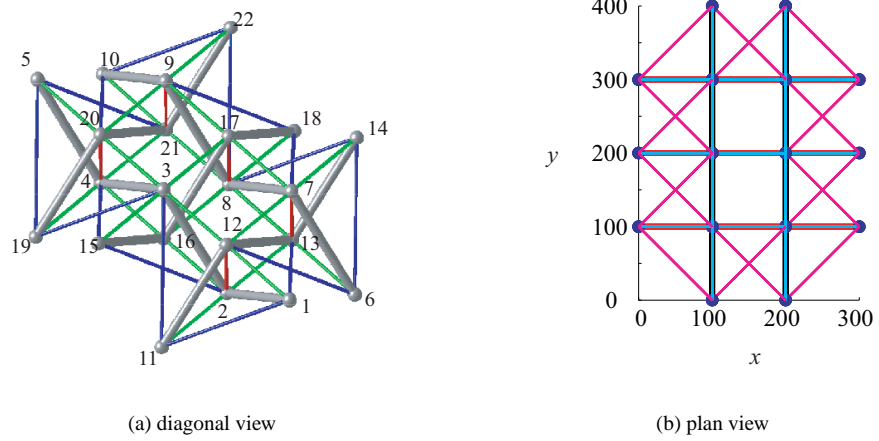


Fig. 7. Tensegrity grid constructed by assembling the unit cell shown in Fig. 8 in  $x$ - and  $y$ -directions.

$10^{-2}, 0.0$ ). Therefore, the ranges  $\delta_\lambda$  and  $\delta_e$  are defined as  $\delta_\lambda = 5.1468 \times 10^{-2}$  and  $\delta_e = 58.534$ . Then, the Pareto optimal solution for  $C = 0.5$  in (32) without uncertainty is found to be  $(\alpha_1, \alpha_2) = (12.591, 12.591)$  with  $(\lambda_{\min}, e) = (0.12386, 14.359)$ , which is shown with 'x' mark in the design variable space in Fig. 6.

The effect of errors in nodal locations with fixed member forces is investigated using this example; i.e., the partial derivatives with respect to nodal locations are investigated, while the variation of member forces are appropriately incorporated through uncertainty in the coefficients of the force modes. The value of  $\lambda_{\min}$  of the deterministic solution with  $C = 0.5$  is 0.12415. If  $z$ -coordinate of node 5 is increased from 40.0 to 41.0, 42.0, 43.0, 44.0, and 45.0, then  $\lambda_{\min} = 0.12394, 0.12372, 0.12350, 0.12328, \text{ and } 0.12305$ , respectively, which means that variation of  $\lambda_{\min}$  is very small for a moderately large variation of nodal location.

Therefore, we consider uncertainty only in member forces. The same range parameter values  $\delta_\lambda = 5.1468 \times 10^{-2}$  and  $\delta_e = 58.534$  are used for this case for comparison purpose between the results with and without uncertainty. Then, the Pareto optimal solution for  $C = 0.5$  is found to be  $(\alpha_1, \alpha_2) = (12.605, 12.639)$  with  $(\tilde{\lambda}_{\min}, \tilde{e}) = (0.12171, 15.855)$ , which is indicated by '+' mark in the design variable space in Fig. 6. Thus,  $\lambda_{\min}$  decreases and  $e$  increases as the result of considering uncertainty. The values of  $(\lambda_{\min}, e)$  at the vertices A, B, C, and D of the region of uncertainty in Fig. 6 are  $(0.12320, 13.654), (0.12171, 13.698), (0.12474, 15.791), \text{ and } (0.12325, 15.855)$ , respectively. Therefore, the minimum value of  $\lambda_{\min}$  and maximum value of  $e$ , i.e., the worst values, are attained at different vertices of the uncertain region.

### 5.3 Example of a tensegrity grid

The tensegrity grid as shown in Fig. 7 [34] is used as the example structure for demonstrating the effectiveness of the proposed method. The structure is constructed by consecutively assembling the unit cell in Fig. 8 in  $x$ - and  $y$ -directions. The thick and thin lines in the figures are struts and cables (or bars), respectively. Note that the members in thin lines that are connected to the boundary nodes do not carry any prestress at the self-equilibrium state; these members are called bars and

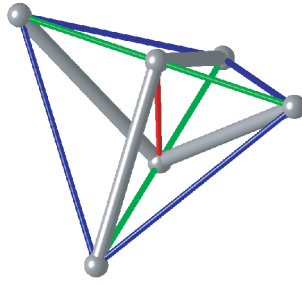


Fig. 8. Unit cell for the tensegrity grid.

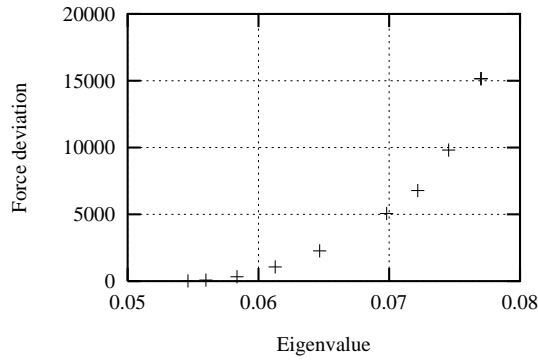


Fig. 9. Pareto optimal solutions in objective function space.

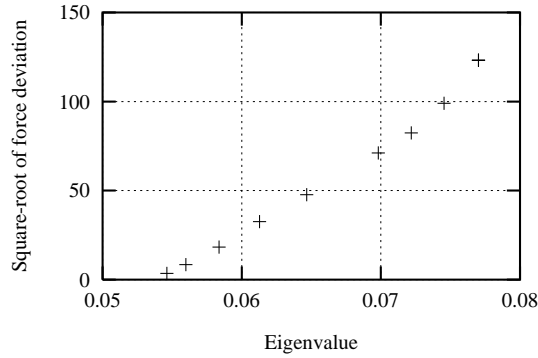


Fig. 10. Relation between minimum eigenvalue and square-root of force deviation of Pareto optimal solutions.

assumed to have stiffness in both of compression and tension in eigenvalue analysis of the tangent stiffness matrix.

Let  $r$  and  $c$  denote the numbers of rows (parallel to  $x$ -axis) and columns (parallel to  $y$ -axis) of the struts, respectively; i.e., there exist  $r + 1$  struts in each column and  $c + 1$  struts in each row. Therefore, the structure has  $2rc + r + c$  struts and  $n = 2(rc + r + c)$  nodes, and the total number of members is  $m = 7rc + 5r + 5c - 4$ . The rank deficiency of the linear stiffness matrix  $\mathbf{K}_E$  after constraining the six rigid-body motions is equal to 1; i.e., this structure has only one infinitesimal mechanism.

The structure in Fig. 7 has three and four struts in  $x$ - and  $y$ -directions, respectively; i.e.,  $r = 3$  and  $c = 2$ . Hence, there are  $m = 63$  members and  $n = 22$  nodes in total. The  $x$ - and  $y$ -coordinates of the nodes are shown in the plan view of the structure in Fig. 7(b), and the height of the grid is 100.

The rank of the equilibrium matrix  $\mathbf{D}$  is  $\kappa = 59$ . Therefore, the structure has four ( $q = 63 - 59 = 4$ ) force modes at the self-equilibrium state, which are denoted by  $\mathbf{g}_1, \dots, \mathbf{g}_4$  with the coefficients  $\alpha = (\alpha_1, \dots, \alpha_4)^\top$ . The bounds  $(s_i^L, s_i^U)$  for the axial forces of the cables and struts are  $(1, 100)$  and  $(-100, -1)$ , respectively. Note that no bound or uncertainty is given for horizontal bars that have vanishing axial force irrespective of the value of  $\alpha$ .

Table 1. Computational cost for enumeration.

Size	$m$	$n$	$q$	$n_c$	$d$	CPU (s)	CPU/ $m^3 \times 10^6$
$(r, c) = (2, 3)$	63	22	4	66	98	0.064	0.256
$(r, c) = (2, 4)$	82	28	5	92	588	0.125	0.227
$(r, c) = (2, 5)$	101	34	6	118	1207	0.256	0.248

The lowest eigenvalue  $\lambda_{\min}$  of  $\mathbf{K}$  is positive at all the vertices after constraining the rigid body motions; i.e., the structure is stable at any set of self-equilibrium forces in the feasible region. The center of the feasible region is computed as  $\alpha^* = (0.4198, 0.5832, 3.2567, 0.4294)^\top$ , which is supposed to be the coefficient vector corresponding to the target axial forces  $\mathbf{s}^*$ .

The values of  $(\lambda_{\min}, e)$  for the single objective problem for maximizing  $\lambda_{\min}$  and minimizing  $e$ , respectively, are  $(0.07701, 1.5160 \times 10^4)$  and  $(0.05461, 1.2723 \times 10^4)$ . Therefore, the ranges  $\delta_\lambda$  and  $\delta_e$  are defined as  $\delta_\lambda = 0.07701 - 0.05461 = 0.02240$  and  $\delta_e = 1.5160 \times 10^4 - 1.2723 \times 10^4 = 0.2437 \times 10^4$ .

The Pareto optimal solutions are found for the weight coefficients  $C = 0.1, 0.2, \dots, 0.9$  in (32), which are plotted in Fig. 9 in the objective function space. In order to see the distribution more clearly, the relation between minimum eigenvalue and square-root of force deviation of Pareto optimal solutions is plotted in Fig. 10. As is seen, the Pareto optimal solutions that form a convex curve in the objective function space have been successfully found using the proposed method.

We next investigate the computational cost for enumeration in the antioptimization process. Computation is carried out using a PC with Intel Core i7 processor (3.97GHz, 6 Cores) and 12 GB RAM. The lower and upper bounds for the forces of cables and struts are relaxed to 0.0. Table 1 shows the size and CPU time for the grids with  $(r, c) = (2, 3)$ ,  $(2, 4)$ , and  $(2, 5)$ , where  $n_c$  is the number of independent linear inequalities, and  $d$  is the number of vertices. As is seen, the number of inequalities  $n_c$  and the number of variables (force modes)  $q$  are proportional to the number of members  $m$ . The CPU time is approximately proportional to  $m^3$ , which is regarded as practically acceptable. Avis and Fukuda [31] theoretically estimated the computational cost for vertex enumeration of polyhedra. In Table 1, the number of variables is much smaller than the number of inequalities, and the computational cost is bounded by the order of  $qm^{q+2}$ . When all vertices are simple (non-degenerate), i.e., the number of active inequalities is not more than  $d$  at each vertex, the order becomes  $qm^{q+1}$ . Note that there are several degenerate vertices in the examples in Table 1. If  $q$  is proportional to  $m$ , then the order becomes exponential function of  $m$ ; however, this is the worst-case estimate of the computational cost. Furthermore, the number of independent force modes is very small for general tensegrity structures; hence, the proposed method is applicable to practical force design problems.

## 6 Conclusions

Properties of Pareto optimal solutions considering the worst-case scenario have been first investigated using a small example of truss optimization for minimum total structural volume and compliance within the framework of NLP. It has been analytically shown that the same set of Pareto optimal solutions for the hybrid optimization-antioptimization problem can be obtained using the linear-weighted-sum approach and constraint approach. This result is not obvious for the case considering the worst-case scenario.

Next, a hybrid approach of multiobjective optimization and antioptimization have been presented for force design of tensegrity structures. The design variables are the coefficients of the self-equilibrium force modes. The objective functions are the lowest eigenvalue of the tangent stiffness matrix and the deviation of forces from the specified target distribution, which are defined as the worst values due to the possible uncertainties in the variables.

The upper-level problem of optimization is solved using an NLP approach, where the sensitivity coefficients are computed by a finite difference approach. The lower-level problems for finding the worst values of objective functions are found using enumeration of the vertices of the uncertain region of the prestresses, which is defined with linear inequalities of the variables. It has been shown in the numerical examples that the Pareto optimal solutions can be successfully found for tensegrity structures by solving the two-level hybrid optimization-antioptimization problem using vertex enumeration combined with an NLP approach.

Note that our approach is concerned with the worst case only, and we do not consider any probabilistic uncertainty. Therefore, statistical evaluation is out-of-scope of the paper. However, our approach is closer philosophically to adopting a uniform distribution as discussed by Elishakoff and Ohsaki [15].

## References

- [1] Motro, R., 1992. "Tensegrity systems: The state of the art". *Int. J. Space Structures*, **7**(2), pp. 75–83.

- [2] Skelton, R. E., and de Oliva, M. C., 2009. *Tensegrity Systems*. Springer, New York.
- [3] Murakami, H., and Nishimura, Y., 2001. "Static and dynamic characterization of some tensegrity modules". *J. Appl. Mech.*, **68**(1), pp. 19–27.
- [4] Crane III, C. D., Duffy, J., and Correa, J. C., 2005. "Static analysis of tensegrity structures". *J. Mech. Des.*, **127**, pp. 257–268.
- [5] Arsenault, M., and Gosselin, C. M., 2005. "Kinematic, static, and dynamic analysis of a planar one-degree-of-freedom tensegrity mechanism". *J. Mech. Des.*, **127**, pp. 1152–1160.
- [6] Coughlin, M. F., and Stamenovic, D., 1997. "A tensegrity structure with buckling compression elements: Application to cell mechanics". *J. Appl. Mech.*, **64**(3), pp. 480–486.
- [7] Cañadas, P., Wendling-Mansuy, S., and Isabey, D., 2006. "Frequency response of a viscoelastic tensegrity model: Structural rearrangement contribution to cell dynamics". *J. Biomechanical Eng.*, **128**, pp. 487–495.
- [8] Connelly, R., 1999. "Tensegrity structures: Why are they stable?". In *Rigidity Theory and Applications*, M. F. Thorpe and P. M. Duxbury, eds. Kluwer/Plenum Publishers, pp. 47–54.
- [9] Tibert, A. G., and Pellegrino, S., 2003. "Review of form-finding methods for tensegrity structures". *Int. J. Space Structures*, **18**(4), pp. 209–223.
- [10] Zhang, J. Y., and Ohsaki, M., 2007. "Optimization methods for force and shape design of tensegrity structures". In Proc. 7th World Congress on Structural and Multidisciplinary Optimization.
- [11] Ohsaki, M., and Zhang, J. Y., 2006. "Stability conditions of prestressed pin-jointed structures". *International Journal of Non-Linear Mechanics*, **41**, pp. 1109–1117.
- [12] Zhang, J. Y., and Ohsaki, M., 2006. "Adaptive force density method for form-finding problem of tensegrity structures". *Int. J. Solids and Structures*, **43**(18–19), pp. 5658–5673.
- [13] Zhang, J. Y., and Ohsaki, M., 2008. "Topology and shape of tensegrity structures". In Proc. 6th Int. Conf. on Computation of Shell and Spatial Structures, IASS-IACM.
- [14] Ben-Haim, Y., and Elishakoff, I., 1990. *Convex Models of Uncertainty in Applied Mechanics*. Elsevier, Amsterdam.
- [15] Elishakoff, I., and Ohsaki, M., 2010. *Optimization and Anti-Optimization of Structures under Uncertainty*. Imperial College Press.
- [16] Ohsaki, M., Zhang, J. Y., and Ohishi, Y., 2008. "Force design of tensegrity structures by enumeration of vertices of feasible region". *Int. J. Space Struct.*, **23**(2), pp. 117–126.
- [17] Ohsaki, M., Zhang, J. Y., and Elishakoff, I., 2008. "Optimization and anti-optimization of forces in tensegrity structures". In Proc. IASS Symposium 2008, Int. Assoc. for Shell and Spatial Struct.
- [18] Cohon, J. L., 1978. *Multiobjective Programming and Planning*. Mathematics in Science and Engineering, 140. Academic Press, New York.
- [19] Marler, T., and Arora, J. S., 2004. "Survey of multi-objective optimization methods for engineering". *Struct. Multidisc. Optim.*, **26**(6), pp. 369–395.
- [20] Massa, F., Lallemand, B., and Tison, T., 2009. "Fuzzy multiobjective optimization of mechanical structures". *Comp. Meth. Appl. Mech. Engng.*, **198**, pp. 631–643.
- [21] Tonon, F., 1999. "Multiobjective optimization of uncertain structures through fuzzy set and random theory". *Computer-Aided Civil and Infrastructure Eng.*, **14**, pp. 119–140.
- [22] Rao, S. S., 1987. "Multi-objective optimization of fuzzy structural systems". *Int. J. Numer. Meth. Eng.*, **24**, pp. 1157–1171.
- [23] Loetamonphong, J., Fang, S.-C., and Young, R. E., 2002. "Multi-objective optimization problems with fuzzy relation equation constraints". *Fuzzy Sets and Systems*, **127**, pp. 141–164.
- [24] Tonon, F., Mammino, A., and Bernardini, A., 2002. "Multiobjective optimization under uncertainty in tunneling: Application to the design of tunnel support reinforcement with case histories". *Tunnelling and Underground Space Technology*, **17**, pp. 33–54.
- [25] Bender, M. J., and Simonovic, S. P., 2000. "A fuzzy compromise approach to water resource systems planning under uncertainty". *Fuzzy Sets and Systems*, **115**, pp. 35–44.
- [26] Zhang, J. Y., Ohsaki, M., and Elishakoff, I., 2010. "Multiobjective hybrid optimization-antioptimization for force design of tensegrity structures". In Proc. 6th China-Japan-Korea Joint Symposium on Optimization of Structural and Mechanical Systems (CJK-OSM6), Paper No. J09.
- [27] Monagan, M. P., Geddes, K. O., Heal, K. M., Labahn, G., Vorkoetter, S. M., McCarron, J., and DeMarco, P., 2004. *Maple 13 Programming Guide*. Maplesoft.
- [28] Horn, R. A., and Johnson, C. R., 1990. *Matrix Analysis*. Cambridge University Press. (Reprint edition).
- [29] Boyd, S., and Vandenberghe, L., 2004. *Convex Optimization*. Cambridge University Press, Cambridge, UK.
- [30] Fukuda, K., 1999. cdd+ Ver. 0.76 User's Manual. Tech. Rep. Technical Report, Inst. Operation Res., ETH-Zentrum, Zurich, Switzerland.
- [31] Avis, D., and Fukuda, K., 1992. "A pivoting algorithm for convex hulls and vertex enumeration of arrangements and polyhedra". *Discrete Comput. Geom.*, **8**, pp. 295–313.

- [32] Avis, D., and Fukuda, K., 1996. "Reverse search for enumeration". *Discrete Applied Math.*, **65**(1–3), pp. 21–46.
- [33] Gill, P. E., Murray, W., and Saunders, M. A., 2002. "SNOPT: An SQP algorithm for large-scale constrained optimization". *SIAM J. Optim.*, **12**, pp. 979–1006.
- [34] Motro, R., 2003. *Tensegrity Structural Systems for the Future*. Butterworth-Heinemann.